Supplementary Information

Photo-coupled electrocatalytic conversion of CO_2-to-CO over cobalt phthalocyanine modified POM-$K_8Ta_6O_{19}$ Z-scheme photocathodes

Chen Liu, Linjie Song, Wanwan Wu, Haiyan Li*, Dongbin Dang*, Yan Bai

Henan Key Laboratory of Polyoxometalate Chemistry, Institute of Carbon Neutrality, College of Chemistry and Molecular Sciences, Henan University, Kaifeng, 475004, China

*Correspondence: **lihaiyan@henu.edu.cn**; dangdb@henu.edu.cn

Experimental procedures

Cobalt phthalocyanine (CoPc) was purchased from Beijing Innochem Science, Nafion solution (5 wt%) was purchased from Sigma-Aldrich, and while $KHCO_3$ and KOH from Kermel. Ta_2O_5 (>99.9%) was bought from Aladdin, and ethanol and isopropyl alcohol were bought from Tianjin Fuyu Fine Chemical. All chemicals were used as received，Milli-Q water (18.2 MΩ) was obtained from ultrapure water system.

Synthesis of Lindqvist type $K_8Ta_6O_{19}\bullet 17H_2O$

The synthesis was performed following a literature method with modifications.[1] Typically, Ta_2O_5 (10 g) was gradually slowly added to a melt of 40 g KOH pellets (85% purity) in a nickel crucible. After heating for 30 min, the melt is cooled to room temperature. Subsequently, 100 mL of high purity water was heated to boiling for degassing, and the coolded melt was dissolved in 100 mL of degassed water. Following, the mixture was filtered through a sand core funnel and the filtrate was concentrated to approximately 25 mL by heating. After keeping at 0° C for 12 h, the resulting crystals were collected by filtration through a sand core funnel, sequentially washed with 1:1 (V/V) ethanol-water mixture and anhydrous ethanol, and finally dried under vacuum.

Synthesis of CoT–*x* Z-scheme heterojunction

$K_8Ta_6O_{19}$ was dispersed in a solution containing anhydrous ethanol and 0.025 g of commercial cobalt phthalocyanine. After severally stirring and sonication for two hours, the anhydrous ethanol was evaporated at 95 °C to obtain a blue solid. Subsequently, the obtained sample was further stabilized at 300 °C for 2 h to form $CoPc/K_8Ta_6O_{19}$, designated as CoT-*x*, where *x* is the mass ratio percentage of $K_8Ta_6O_{19}$ to CoPc.

Fabrication of CoT-*x* Z-scheme heterojunction photocathodes

A mixture of 8 mg of catalyst, 3.5 mg of carbon black, 240 μL of high purity water, 240 μL of isopropanol and 160 μL of 5% Nafion solution was prepared as a catalyst suspension. The prepared slurry was sonicated for 2 h and then drop-cast uniformly onto hydrophobic carbon paper within a defined area of 1 × 2cm^2. The carbon paper coated catalyst, where the amount of the catalyst loaded was controlled to be

approximateiy 0.35 mg cm^{-2}, was then dried overnight in a vacuum oven at 60°C.

Photoelectrochemical and CO_2 reduction properties measurements

The photoelectrochemical/electrochemical tests of all the photocathodes were performed on an electrochemical workstation (CHI760E) by a H-cell (separated from a Nafion D-115 cation exchange membrane) using a three-electrode system of CoT-*x*|Ag/AgCl|Pt, where Pt sheet and Ag/AgCl were used as counter and reference electrodes, respectively, and the as-fabricated CoT-*x* catalysts coated on carbon paper were used as working electrode. A 300 W xenon lamp served as a light source in this study. The light intensity was set at approximately 16 mW/cm^2 and xenon lamp positioned 20 cm from the reaction window. All potentials were calibrated by the Nernst equation to the reversible hydrogen electrode (RHE) reference scale using $E_{RHE} = E_{Ag/AgCl}+0.059\times pH + 0.197$. 0.5 M $KHCO_3$ was used as the electrolyte solution for the photoelectrocatalytic CO_2 reduction measures, and it needed to be purged with high-purity CO_2 (99.99 %) gas for at least 30 min before the test to reach saturation. After CO_2 saturation, a pH value of 7.2 can be obtained for the electrolyte. The achieved gaseous products at each fixed potential were analyzed using gas chromatography (Panna A91 Plus GC) equipped with a flame ionization detector (FID) and a thermal conductivity detector (TCD). High-purity argon gas (Ar, 99.99 %) was used as the carrier gas. During the measures, the flow rate of the CO_2 gas was controlled by a Sevenstar D07－7 mass flow controller to be 14 standard cubic centimeters per minute (sccm). Scan activation was performed at a scan rate of 0.05 V s^{-1} for 20 cycles of cyclic voltammetry (CV). Liquid products were analyzed by ^1H NMR (Bruker, Switzerland).

Catalysts characterization

The crystalline structures of all catalysts were identified by X-ray diffraction (XRD, Bruker D8 advance diffractometer, Germany) using Cu Kα radiation (λ= 0.15406 nm). The morphology of the samples was observed by a field emission scanning electron microscope (FESEM, JSM-7610F, Japan) and a high-resolution transmission electron microscope (HRTEM, FEI Tecnai G2 F20, America). ^1H NMR spectra were recorded

on an ASCEND 500 BRUKER with D_2O as the solvent at room temperature. Chemical shifts are reported in ppm, and coupling constants are given in Hz. X-ray photoelectron spectroscopy (XPS) measurements were performed using an ESCALAB 250 Xi spectrometer (USA) with Al-Kα radiation to analyze the surface electronic states of the catalysts, here, the samples were prepared by pelletizing the powder. The XPS survey spectrum and fine spectrum were detected using a pass energy of 100 eV and 30 eV, respectively. The detection pressure is $8' 10^{-10}$ mBar. The binding energy was calibrated by referencing the C 1s peak at 284.8 eV as the reference. The UV-vis diffuse reflectance spectroscopy of the catalysts were determined with $BaSO_4$ as the reference at room temperature by using a UV-vis spectrophotometer (Agilent Cary 5000, USA). Inductively coupled plasma optical emission spectroscopy (ICP-OES, America Agilent 5110) was used to analyze the element composition of the sample quantitatively. The photoluminescence spectra (PL) measurements were carried out on a spectrophotometer (F7000, Japan) with an excitation wavelength of 430 nm. The electron paramagnetic resonance (EPR) signal of oxygen vacancy was recorded by Bruker 300 EPR spectrometer at 77 K. The Fourier transform infrared spectra (FT-IR, Spectrum Two, America) of the samples were recorded from 400 to 4000 cm^{-1} using KBr pellets in a spectrometer. In situ attenuated total reflectance FTIR (ATR-FTIR) were employed to gain a better insight into the PEC CO_2 reaction mechanism on a Thermo Nicolet 8700 spectrometer equipped with an MCT detector. Chemical deposition of Au thin film (~60 nm) on the Si prism was prepared according to a "two-step wet process". The catalyst suspensions were dropped on the Au/Si surface as the working electrode. The mass loading of the catalyst was 0.35 mg cm^{-2}, and the electrolyte was 0.5 M $KHCO_3$. In situ FT-IR spectra were recorded during the stepping of the working electrode potential. Raman spectra were recorded on a laser micro Raman spectrometer (British Renishaw inVia).

Faradaic efficiency (FE)[2]

$$FE(CO) = \frac{N_f}{N_{total}} = \frac{x_0 \times N_A \times n \times P \times v \times 1.602 \times 10^{-19}}{I_0 \times R \times T} \times 100\%$$

N_f: Number of electrons required to produce f

N_{total}: Total number of electrons for CO_2 reduction

x_0: Where x_0 is the concentration (ppm) of the achieved product *f*

N_A: Avogadro constant, 6.02×10^{23}

n: number of transferred electrons (for H_2 and CO, n=2)

v: the flow rate of the CO_2 gas

I_0: current at injecting moment

R: Molar gas constant, 8.314 J/ mol× K

TOF calculations. The TOF was calculated through the following equation[3]

$$TOF(h^{-1}) = \frac{I_{product}/nF}{\alpha \times m_{cat}/M_{metal}} \times 3600$$

$I_{product}$: partial current density for CO

n: number of electrons transferred for CO_2 to CO, 2

F: Faradaic constant, 96485 C/mol

m_{cat}: catalyst mass in the electrode

α: mass ratio of active atoms in the catalyst

M_{metal}: atomic mass of metal

Kubelka-Munk functio:[4]

$$(\alpha hv)^2 = A(hv - Eg)$$

α: absorption coefficient

h: Planck's constant

v: optical frequency

A: constant

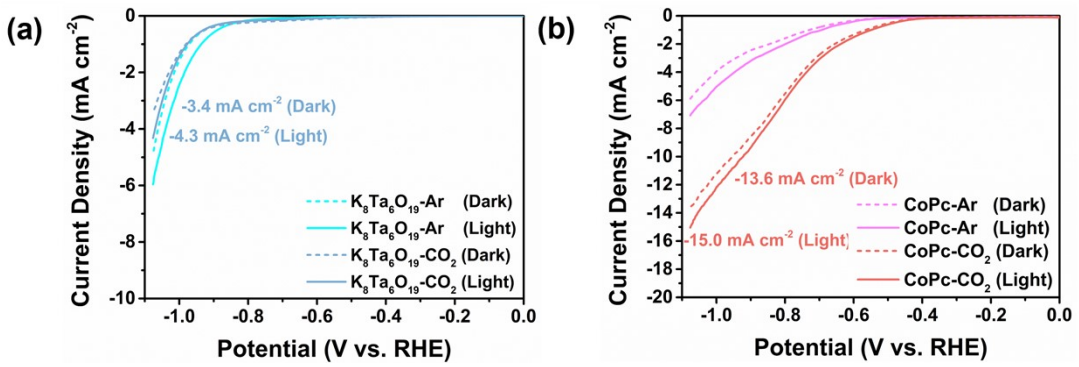

Fig. S1 LSV curves of (a) CoPc, (b) $K_8Ta_6O_{19}$. The dotted lines represent the condition without light (EC) and the solid lines represent the condition with light (PEC).

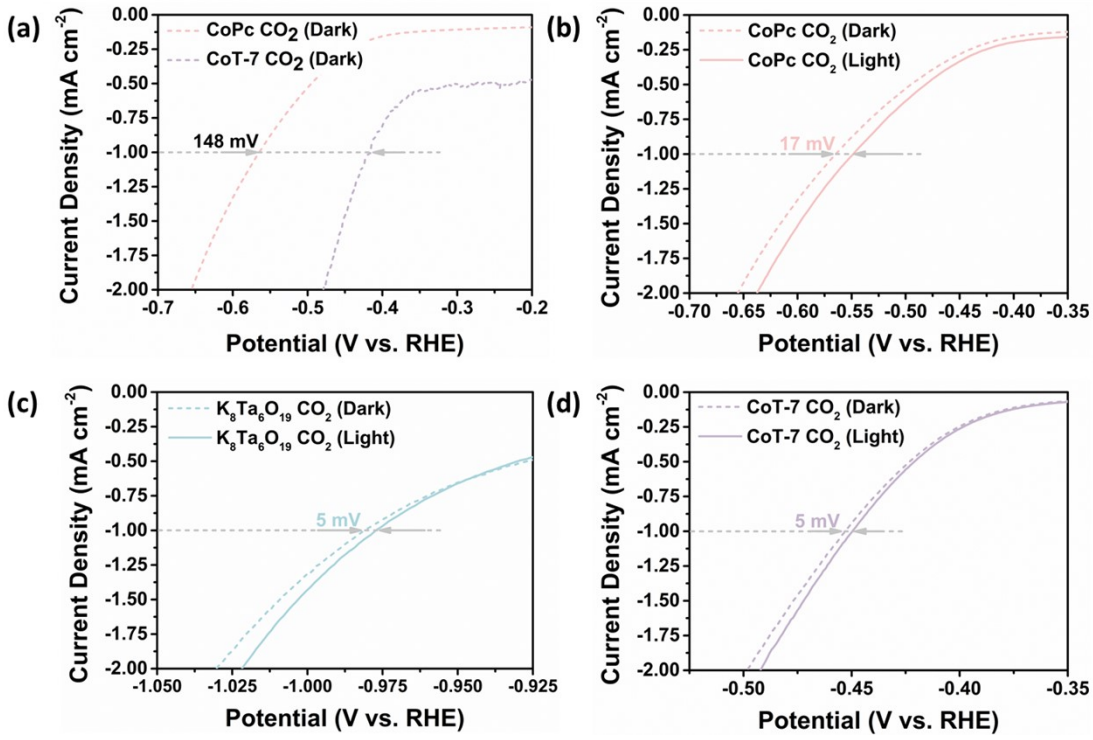

Fig. S2 (a) CoPc and CoT-7 heterogeneous change of the onset potential (1 mA cm^{-2}) in CO_2-saturated 0.5 M $KHCO_3$; LSV curves of (b) $K_8Ta_6O_{19}$, (c) CoPc, and (d) CoT-7 heterogeneous. The change of the onset potential (1 mA cm^{-2}) after illumination in CO_2-saturated 0.5 M $KHCO_3$.

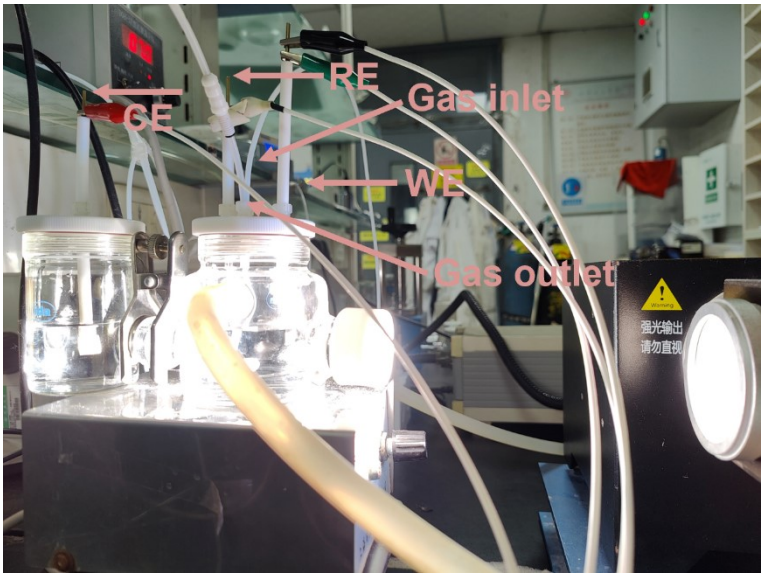

Fig. S3 H-type electrolytic cell used for photoelectrocatalytic CO_2 reduction.

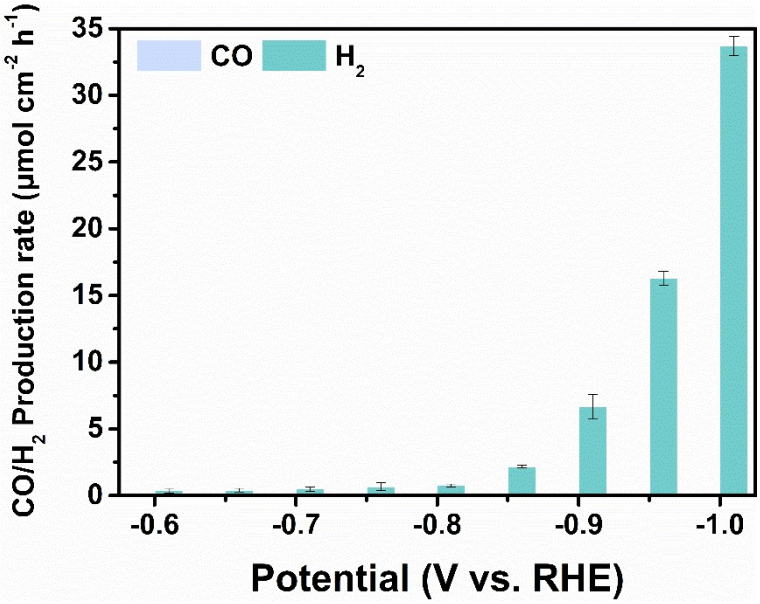

Fig. S4 CO/H_2 production rate of $K_8Ta_6O_{19}$.

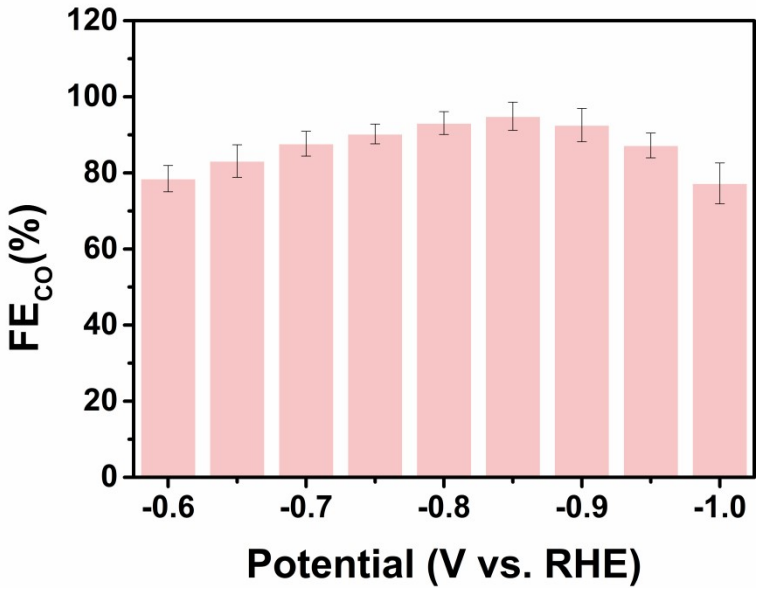

Fig. S5 CO Faraday efficiency over CoPc under illumination.

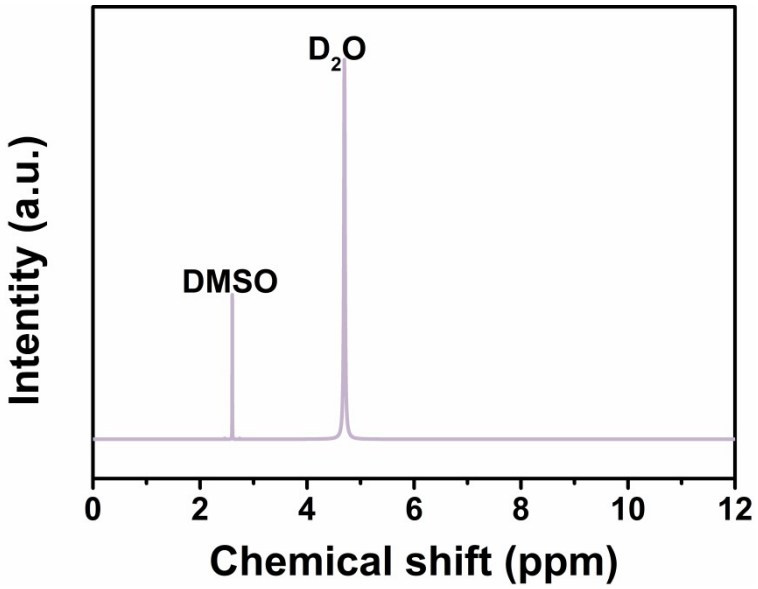

Fig. S6 ^{1}H NMR singles of CO_2 reduction on CoT-7 catalyst.

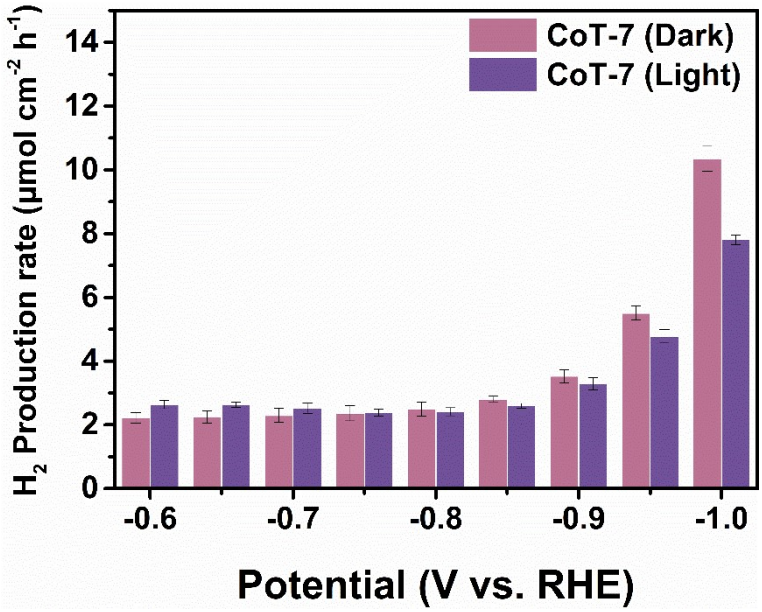

Fig. S7 H_2 production rates of CoT-7 under dark and light conditions in CO_2 atmosphere.

Table S1. Different Co atom loadings on CoT-7 heterojunction and CoPc.

Photo-copled electrocatalysts	Co atom loading (%)
CoPc	10.07
CoT-7 heterojunction	1.2

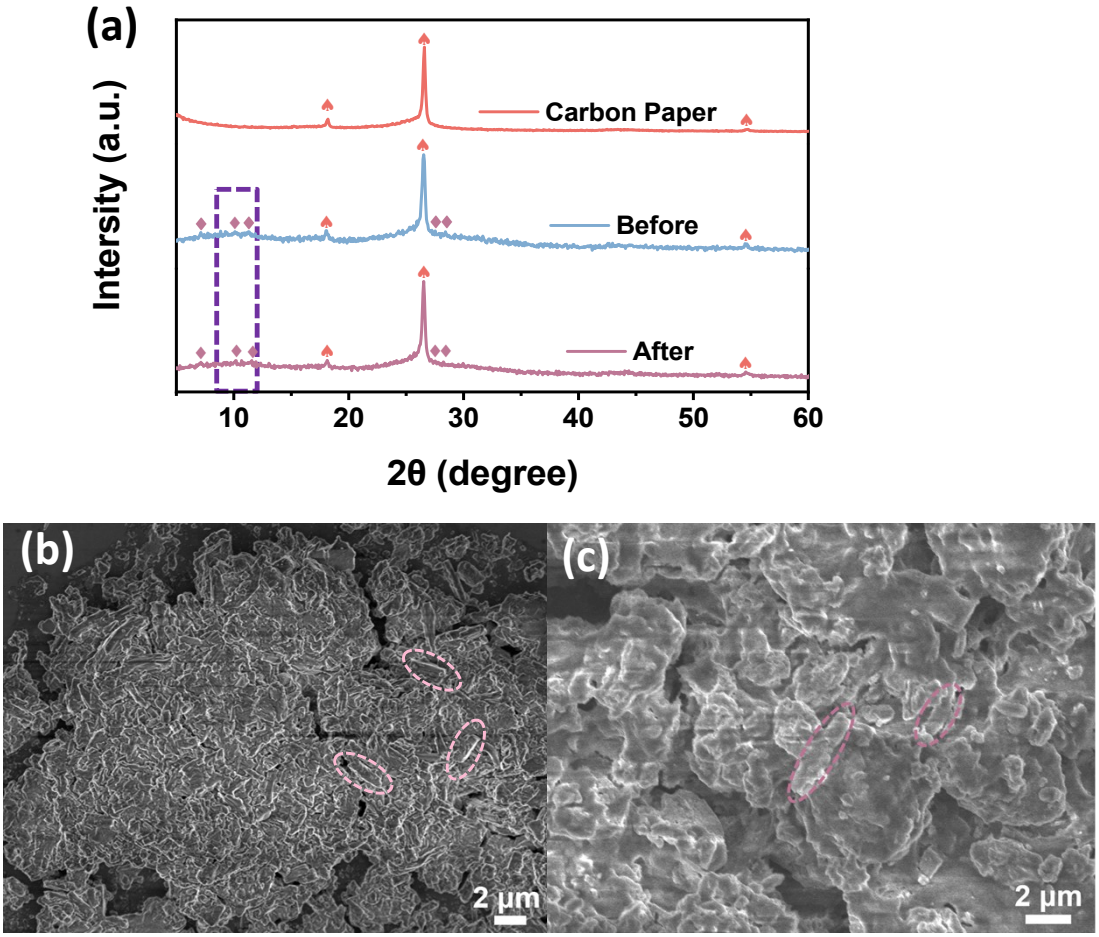

Fig. S8 (a) XRD patterns of CoT-7 coated on the carbon paper before and after reaction (♦: CoT-7, ♠: Carbon Paper); (b) (c) FESEM images of CoT-7 before and after reaction.

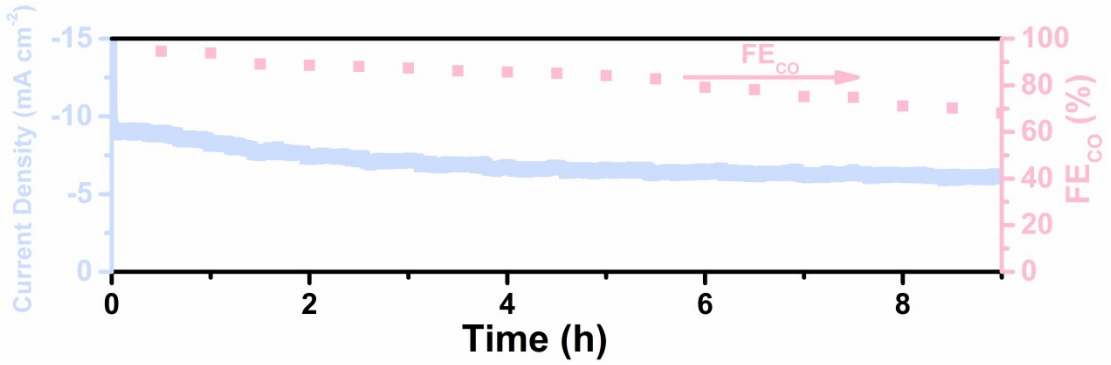

Fig. S9 Stability test chart of CoPc.

Table S2. CO_2RR performance comparison of CoT-7 heterojunction with other reported catalysts in aqueous solution.

Catalysts	Potential (V vs. RHE)	j_{CO} (mA cm^{-2})	FE_{CO} (%)	Reference
CoT-7 heterojunction (Light)	**-0.9**	**25.8**	**99.56**	**This work**
CoT-7 heterojunction (Dark)	**-0.9**	**24.6**	**98.1**	**This work**
Cu_{SA}@AHPC	-0.6	3.48	96.1%	5
Zn@ZnO-T	− 1.2	12.75	92.1%	6
MXene@Por-COF-Co-7	-0.6	9.33	97.28	7
CNT-UrFe	−0.78	1.62	99.9	8
Se-CNs	-0.6	9.1	90%	9
CoPc-PI-COF-1	−0.90	21.2	95	10
$SnSe_2$-graphene nanosheets	-0.9	11.8	95.1%	11
Cu-In_2O_3/C	−0.48	0.55	86.7%	12
Crumpled Pd(100) surface	-0.59	6.6	93%	13
GaN (Light)	0.17	18	65	14
$Cu_2O/Ga_2O_3/TiO_2$ (Light)	0.44	1.18	22.67	15
Co-qPyH/TiO_2/CIGS (Light)	0.2	3.0	89	16
Au_3Cu NPs/Si NW (Light)	-0.2	2.2	80	17
nanoporous Au mesh	-0.03	2.94	91	18

on Si (Light)				
Al-PMOF(Co) (Light)	-0.8	4.3	90	19
Zn-CoTAPc/PMo_{12} MLSs (Light)	-0.75	18.7	96.2	20
CoN-7 heterojunction (Light)	-0.85	16.4	98.6	21

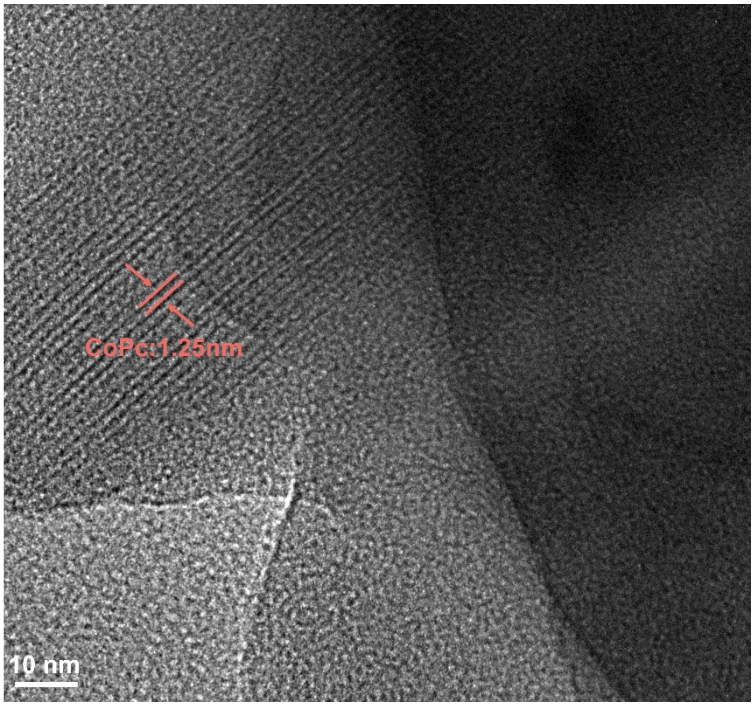

Fig. S10 High-resolution TEM images of CoPc.

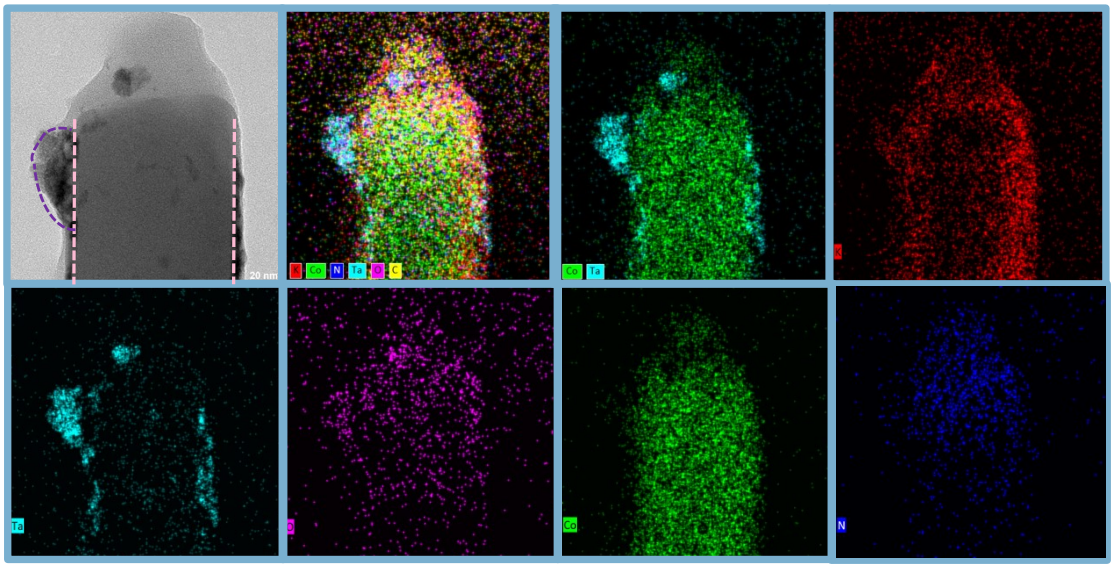

Fig. S11 High-resolution TEM images and mappings of CoT-7.

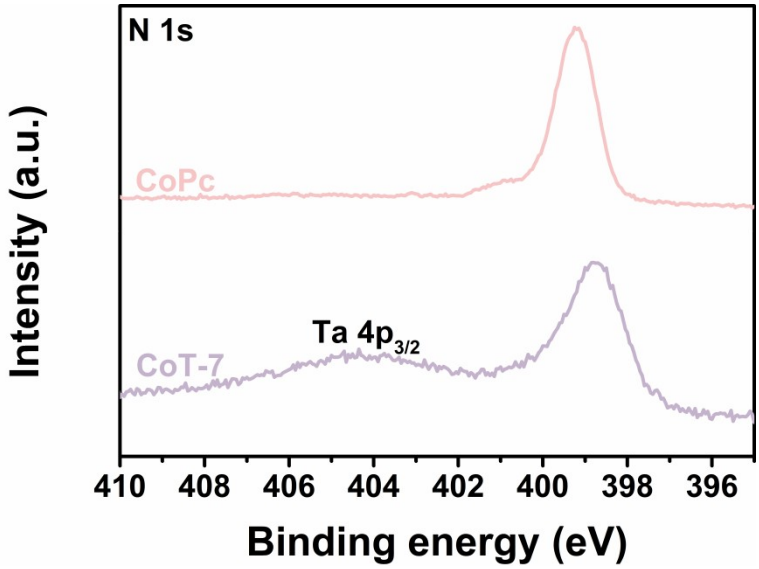

Fig. S12 N 1s high resolution XPS spectra.

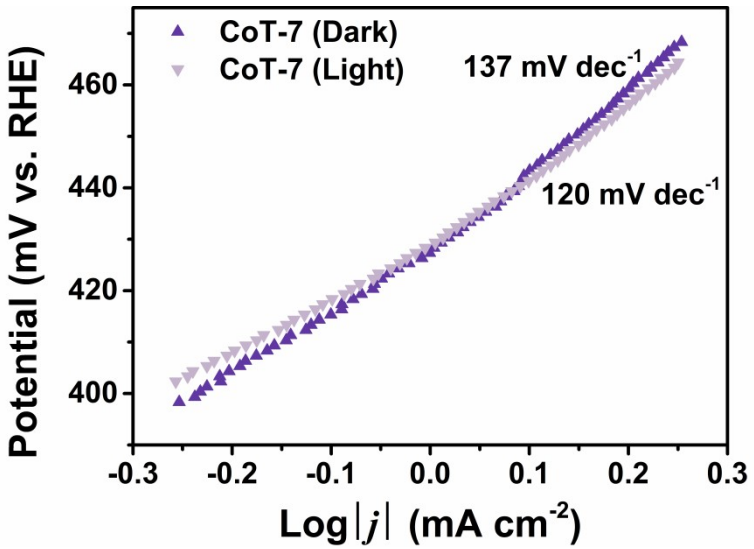

Fig. S13 Tafel slope plots of CoT-7.

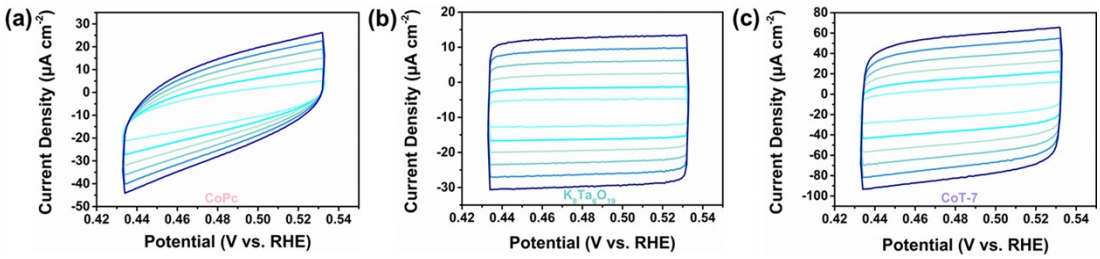

Fig. S14 Cyclic voltammograms (CV) curves under different scan rates for $K_8Ta_6O_{19}$, CoPc, and CoT-7 heterojunction.

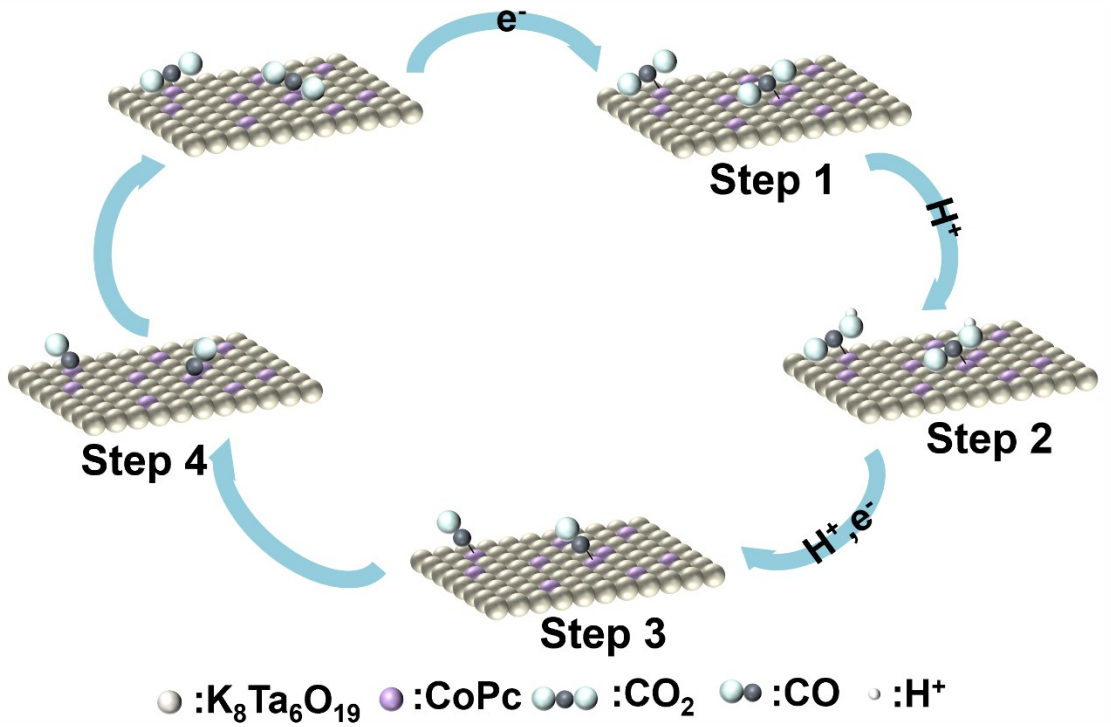

Fig. S15 The CO_2-to-CO conversion reactive pathway and intermediate architectures over CoT-7 heterojunction.

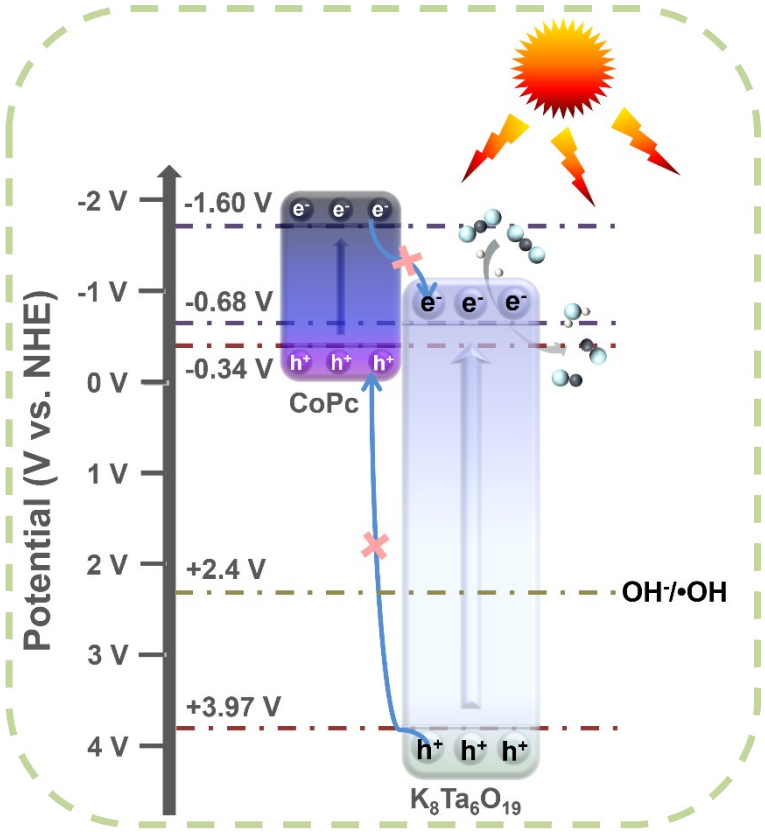

Fig. S16 Type-II mechanism for PEC reduction of CO_2 into chemical fuels.

References：

1 S. Li, S. Chen, F. Zhang, Z. Li, C. Zhang, G. Cao and B. Zhai, Synthesis and characterization of two polyoxotantalates: A building block and its dimeric. *Inorganic Chemistry Communications*, 2019, **106**, 228–232.

2 Q. Zhang, D. Ren, S. Pan, M. Wang, J. Luo, Y. Zhao, M. Grätzel and X. Zhang, Micro-Electrode with Fast Mass Transport for Enhancing Selectivity of Carbonaceous Products in Electrochemical CO_2 Reduction. *Adv Funct Materials*, 2021, **31**, 2103966.

3 S. Chen, X. Li, C. Kao, T. Luo, K. Chen, J. Fu, C. Ma, H. Li, M. Li, T. Chan and M. Liu, Unveiling the Proton-Feeding Effect in Sulfur-Doped Fe-N-C Single-Atom Catalyst for Enhanced CO_2 Electroreduction. *Angew Chem Int Ed*, 2022, **61**, e202206233.

4 W. Wang, Q. Song, C. Liu, H. Li, Y. Bai and D. Dang, Highly efficient photocatalytic environmental remediation of MET over Z-Co_3O_4/$K_7HNb_6O_{19}$ Z-scheme heterojunction with controllable hierarchical peony flower-like morphology using Co-ZIF-67 as a template. *Applied Surface Science*, 2023, **630**, 157447.

5 C. Wang, K. Zhang, X. Zhang, J. Wang, X. Luo, G. Li and K. Wang, Zwitterionic polymer-assisted asymmetrically coordinated Cu atoms on aligned carbonous microchannels for efficient electroreduction of CO_2 to CO†. *Green Chem.*, 2025, **27**, 5236–5245.

6 X. Liu, J. Ge, S. Li, H. Yang, H. Tian, H. Liu, Y. Li, X. Zheng, Y. Tian, X. Cui and Q. Xu, Activating dynamic Zn–ZnO interface with controllable oxygen vacancy in CO2 electroreduction for boosting CO production†. *Green Chem.*, 2025, **27**, 6133–6144.

7 L. Zhou, Q. Tian, X. Shang, Y. Zhao, W. Yao, H. Liu and Q. Xu, Heterostructure construction of covalent organic frameworks/Ti_3C_2-MXene for high-efficiency electrocatalytic CO2 reduction†. *Green Chem.*, 2024, **26**, 1454–1461.

8 C. Zhang, D. Dragoe, F. Brisset, B. Boitrel, B. Lassalle-Kaiser, W. Leibl, Z. Halime and A. Aukauloo, Second-sphere hydrogen-bonding enhances heterogeneous electrocatalytic CO_2 to CO reduction by iron porphyrins in water†. *Green Chem.*,

2021, **23**, 8979–8987.

9 B. Zhang, J. Zhang, F. Zhang, L. Zheng, G. Mo, B. Han and G. Yang, Selenium-Doped Hierarchically Porous Carbon Nanosheets as an Efficient Metal-Free Electrocatalyst for CO_2 Reduction. *Adv Funct Materials*, 2020, **30**, 1906194.

10 B. Han, X. Ding, B. Yu, H. Wu, W. Zhou, W. Liu, C. Wei, B. Chen, D. Qi, H. Wang, K. Wang, Y. Chen, B. Chen and J. Jiang, Two-Dimensional Covalent Organic Frameworks with Cobalt(II)-Phthalocyanine Sites for Efficient Electrocatalytic Carbon Dioxide Reduction *J. Am. Chem. Soc.*, 2021, **143**, 7104–7113.

11 S. Shao, T. Wen, Z. Wang, X. Yin, Y. Liu, W. Yang and Y. Chen, Fabrication of $SnSe_2$-graphene nanosheets for highly effectively electrocatalytic reduction of CO_2. *Electrochimica Acta*, 2022, **434**, 141331.

12 Y. Ye, Y. Liu, Z. Li, X. Zou, H. Wu and S. Lin, Highly selective and active Cu-In_2O_3/C nanocomposite for electrocatalytic reduction of CO_2 to CO. *Journal of Colloid and Interface Science*, 2021, **586**, 528–537.

13 Y. Zhao, X. Tan, W. Yang, C. Jia, X. Chen, W. Ren, S. C. Smith and C. Zhao, Surface Reconstruction of Ultrathin Palladium Nanosheets during Electrocatalytic CO_2 Reduction. *Angew Chem Int Ed*, 2020, **59**, 21493–21498.

14 S. Chu, P. Ou, R. T. Rashid, P. Ghamari, R. Wang, H. N. Tran, S. Zhao, H. Zhang, J. Song and Z. Mi, Decoupling Strategy for Enhanced Syngas Generation from Photoelectrochemical CO_2 Reduction. *iScience*, 2020, **23**, 101390.

15 M. Xia, L. Pan, Y. Liu, J. Gao, J. Li, M. Mensi, K. Sivula, S. M. Zakeeruddin, D. Ren and M. Grätzel, Efficient Cu_2O Photocathodes for Aqueous Photoelectrochemical CO_2 Reduction to Form at eand Syngas. *J. Am. Chem. Soc.*, 2023, **145**, 27939–27949.

16 P. B. Pati, R. Wang, E. Boutin, S. Diring, S. Jobic, N. Barreau, F. Odobel and M. Robert, Photocathode functionalized with a molecular cobalt catalyst for selective carbon dioxide reduction in water. *Nat Commun*, 2020, **11**, 3499.

17 Q. Kong, D. Kim, C. Liu, Y. Yu, Y. Su, Y. Li and P. Yang, Directed Assembly of Nanoparticle Catalysts on Nanowire Photoelectrodes for Photoelectrochemical CO_2 Reduction. *Nano Lett.*, 2016, **16**, 5675–5680.

18 J. T. Song, H. Ryoo, M. Cho, J. Kim, J. Kim, S. Chung and J. Oh, Nanoporous Au Thin Films on Si Photoelectrodes for Selective and Efficient Photoelectrochemical CO_2 Reduction. *Advanced Energy Materials*, 2017, **7**, 1601103.

19 K. Wang, Y. Liu, J. Kang, Y. Zhang, Q. Wang, L. Chen, Q. Wang, B. Liu, M. Liu, X. Qiu, W. Li and J. Li, Site-selective photocoupled electrocatalytic CO_2 reduction over efficient Al-oxo chain based-porphyrin framework. *Applied Catalysis B: Environmental*, 2023, **325**, 122315.

20 H. Yang, D. Yang, Y. Zhou and X. Wang, Polyoxometalate Interlayered Zinc−Metallophthalocyanine Molecular Layer Sandwich as Photocoupled Electrocatalytic CO_2 Reduction Catalyst. *J. Am. Chem. Soc.*, 2021, **143**, 13721–13730.

21 C. Liu, Z. Bian, W. Wang, H. Li, D. Dang and Y. Bai, Photoelectrochemically converting CO_2 over Z-scheme heterojunction CoPc/$K_7HNb_6O_{19}$ with high Faraday efficiency. *Applied Surface Science*, 2024, **663**, 160192.